Supramolecular Ring Banded Prototype Liquid Crystalline Oligo(phenylenevinylene)

S. R. Amrutha[†] and M. Jayakannan*[,‡]

Chemical Sciences & Technology Division, National Institute for Interdisciplinary Science and Technology, Thiruvananthapuram 695019, Kerala, India, and Department of Chemistry, Indian Institute of Science Education and Research (IISER), NCL Innovation Park, Dr. Homi Bhabha Road, Pune 411008, India

Received: November 12, 2008; Revised Manuscript Received: February 18, 2009

We report a new ring banded supramolecular structure in thermotropic liquid crystalline oligo(phenylenevinylene) (OPV) via a melt crystallization process. A series of structurally different OPV molecules were synthesized using tricyclodecanemethanol (TCD) as a bulky pendant unit to trace ring banded morphology. Among all, an OPV molecule with rigid bis-TCD units in the central core and flexible dodecyl chains at the outer phenyl rings (BTCD-BDD-OPV) was found to show ring banded morphologies, which is a first of its kind in π-conjugated materials. BTCD-BDD-OPV experiences strong aromatic $\pi-\pi$ interactions in both film and liquid crystalline (LC) frozen stage. The π-induced aggregation leads to lamellar self-assembly of OPV-mesogens that subsequently undergo helical crystal growth, thereby producing dark and bright ring banded patterns. Variable temperature X-ray diffraction analysis revealed the existence of three peaks at 27.07, 13.97, and 8.90 Å corresponding to 001, 002, and 003 fundamental layers, respectively, thus confirming the lamellar self-assembly of OPV-mesogens. Electron microscopic (SEM and TEM) analysis of the LC frozen sample showed images confirming helical microcrystalline assembly and providing direct evidence for the self-organization mechanism. Detailed photophysical experiments such as excitation, emission, and time-resolved fluorescence decay studies indicated that BTCD-BDD-OPV has very strong $\pi-\pi$ interaction in both film and LC frozen stage, which was found to be main driving force for the formation of supra-ring structure. Upon illumination with light, the OPV chromophores in the LC phase were excited and the color of the samples turned into luminescent green ring bands.

Introduction

Crystallization is one of the most fundamental phenomena that is studied in solids and semicrystalline polymers because of its close association with macroscopic properties such as mechanical strength and thermal transitions. Crystallization consists of two consecutive steps, nucleation and crystal growth. Though nucleation is highly dependent on the nature of the material, crystal growth appears to be the most important step for the observation of morphological features in all crystalline materials. One of the widely observed features in the morphology of crystalline material (including polymers) is the appearance of micrometer-range spherulites.[1] Liquid crystalline (LC) materials belong to another class of crystalline solids, and their morphologies are, in general, completely different from normal spherulites depending on their LC state, such as nematic, smectic, and cholestric, etc.[2] Recently, a new type of ring banded spherulitic structure was reported in commercial semicrystalline polymers during their crystallization from the melt.[3,4] Keith et al. and few others had carried out detailed studies on the mechanism of formation of these ring banded structure using theoretical and microscopic studies and computational simulations.[5−10] The origin of the ring banded structure is generally accepted to be the periodic twisting of lamellar crystals along the radial growth direction of the spherulites.[11−13] The lamellar twisting phenomenon was correlated to surface stress,[14] chain folding direction of the crystal growth,[15] periodic change of concentration gradient,[16] and also the segregation of amorphous polymer chains from the crystal fronts of polymer binary blends.[3,17−20] Though the twisting of the lamellar crystal mechanism was widely accepted in all of these cases, there seems to be no correlation between the structure of the materials (polymers or small molecules) and appearance of ring banded patterns. It is also important to note that different types of mechanisms were proposed for various materials and there is no common explanation for the formation of banded spherulites with respect to their chemical structures.

Noncovalent interactions such as hydrogen bonding and $\pi-\pi$ stacking of aromatic cores have been employed as tools to self-assemble molecular building blocks to produce relatively large and defect-free supramolecular architectures.[21−25] These supramolecular structures were most often visualized as macroscopic properties such as liquid crystalline, viscous mass, or reversible/irreversible molecular gels.[26−32] Liquid crystalline supramolecular materials were particularly very promising because of their potential applications in light-emitting diodes,[33] photovoltaic cells,[34] field-effective transistors,[35] chemical and biosensors,[36] etc. Owing to their large complexity, oligomers of semiconducting polymers have been utilized as molecular skeletons for self-assembly rather than the large macromolecular (or polymer) chains. Oligo(phenylenevinylene)s (OPVs) are one of the widely studied π-conjugated systems due to their good emission and charge transport properties.[37] Hydrogen bond inducing skeletons have been attached in the OPV backbone, and both H-bonding and aromatic π-stacking interactions have been utilized for supramolecular LC materials.[38,39] Jonkheijm et al. reported spectroscopic investigation of hydrogen-bonded OPV derivatives and found that an organized shell of solvent

* To whom correspondence should be addressed. E-mail: jayakannan@iiserpune.ac.in. Fax: 0091-20-25898022

[†] National Institute for Interdisciplinary Science and Technology.

[‡] Indian Institute of Science Education and Research.

10.1021/jp809994t CCC: $40.75
Published on Web 03/20/2009

SCHEME 1: Synthesis and Structure of Bulky Oligo(phenylenevinylenes)

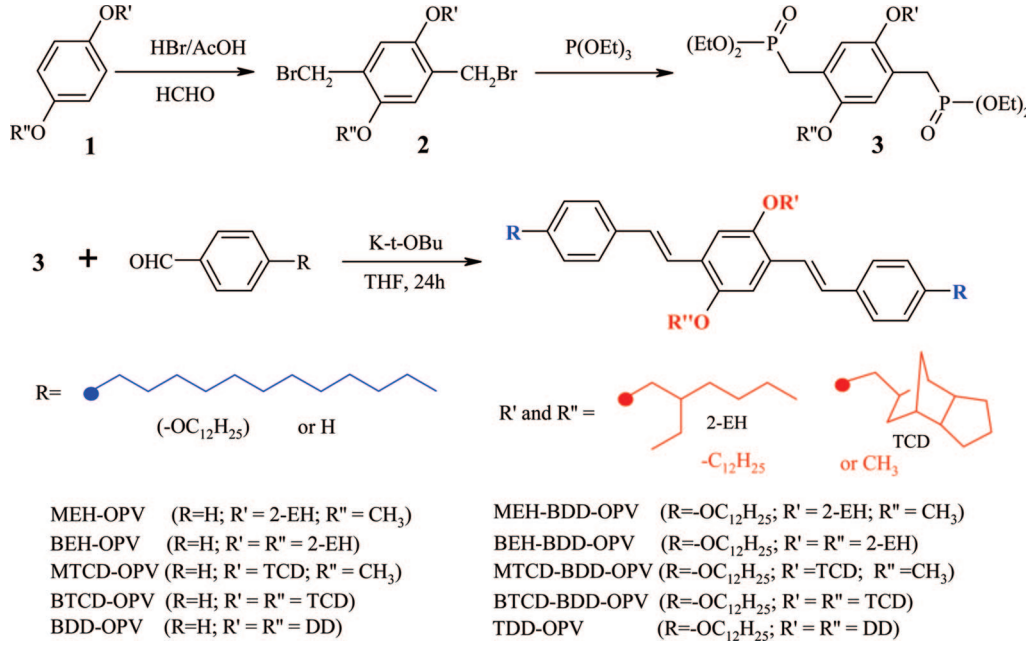

MEH-OPV (R=H; R' = 2-EH; R" = CH_3)
BEH-OPV (R=H; R' = R" = 2-EH)
MTCD-OPV (R=H; R' = TCD; R" = CH_3)
BTCD-OPV (R=H; R' = R" = TCD)
BDD-OPV (R=H; R' = R" = DD)

MEH-BDD-OPV (R=-$OC_{12}H_{25}$; R' = 2-EH; R" = CH_3)
BEH-BDD-OPV (R=-$OC_{12}H_{25}$; R' = R" = 2-EH)
MTCD-BDD-OPV (R=-$OC_{12}H_{25}$; R' =TCD; R" =CH_3)
BTCD-BDD-OPV (R=-$OC_{12}H_{25}$; R' = R" = TCD)
TDD-OPV (R=-$OC_{12}H_{25}$; R' = R" = DD)

molecules played a major role toward self-assembly.[40] A few reports have been published for the effect of alkyl side chains, increase in the chain length, or fluoro-substitution on the LC properties of OPVs.[41−44] Most of the conducting polymers or oligomer-based LC materials were generally found to be nematic, smectic, or columnar liquid crystalline materials. π-Conjugated ring banded suprastructures would be very attractive since patterning of electronic materials could be achieved via a melt crystallization process. The idea of studying a fundamental phenomenon such as ring banded structure formation in a system like a luminescent OPV is very stimulating because (i) it provides a new opportunity to trace the molecular interactions and factors that directly influence the mechanism of the formation of ring bands and (ii) the resultant ring banded luminescent materials could be a new entry into opto-electronic materials that are attractive alternatives for new applications.

Here, we have designed and synthesized a series of more than 10 bulky OPV molecules for tracing the ring banded structure formation in a LC π-conjugated system (see Scheme 1). All of the OPVs had in common three aromatic units that differed in the nature of the pendants either in the middle or the outer phenyl rings. A bulky pendant, 1,8-tricyclodecanemethanol (TCD), has been utilized for making the bulky conjugated OPVs.[45−47] Both isothermal and non-isothermal crystallization processes were employed as tools to study the ring banded structures. Electron microscopic (SEM and TEM) analysis and variable temperature X-ray diffraction studies were carried out in the LC samples to identify lamellar twisting and the mechanism of ring banded structures. Detailed photophysical studies (excitation, emission, and time-resolved fluorescence decay studies) were carried out in both film and LC frozen samples to trace the role of $\pi-\pi$ interactions in OPV mesogens for the ring banded structure formation.

Experimental Methods

Materials. 1,8-Tricyclodecanemethanol was donated by Celanese Chemicals & Co. and used without further purification. *p*-Toluenesulfonylchloride, 4-methoxyphenol, hydroquinone, 2-ethylhexylbromide, potassium *tert*-butoxide (in 1 M THF solution,) and quinine sulfate were purchased from Aldrich Chemicals. HBr in glacial acetic acid, paraformaldehyde, and all other reagents/solvents were purchased locally and purified by following the standard procedures. 1,4-Bis(bromomethyl)-2-methyloxy-5-(2-ethylhexyloxy)benzene, 1,4-bis(bromomethyl)-2,5-di(2-ethylhexyloxy)benzene, 1,4-bis(bromomethyl)-2-methyloxy-5-(1,8-tricyclodecanemethyleneoxy)benzene, 1,4-bis(bromomethyl)-2,5-di(1,8-tricyclodecanemethyleneoxy)benzene, 1,4-bis(bromomethyl)-2,5-di(dodecyloxy)benzene,[48] and their corresponding ylides were synthesized according to reported procedures.[45,46]

General Procedures. ^{1}H and ^{13}C NMR spectra of the compounds in $CDCl_3$ containing small amount of TMS as internal standard were recorded using a 300-MHz Bruker NMR spectrophotometer. Infrared spectra of the samples were recorded with a Perkin-Elmer Fourier transform infrared (FTIR) spectrophotometer in the solid state. The purity of the compounds was determined by JEOL JSM600 fast atom bombardment (FAB) high-resolution mass spectrometry. The compound was dissolved in $CHCl_3$ and suspended in 3-nitrobenzylalcohol as a matrix for FAB mass measurements. Elemental analysis of the compounds was carried out using a Perkin-Elmer Series II CHNS/O Analyzer 2400. The thermal stability of the oligophenylenevinylenes was determined using a DTG-60 Shimadzu thermogravimetric analyzer at a heating rate of 10 °C/min in a nitrogen atmosphere. Thermal analyses of the polymers were performed with a Perkin-Elmer Pyris-6 differential scanning calorimetry (DSC) instrument under nitrogen, and the instrument was calibrated with indium, tin, and lead standards. All samples were first heated to melt prior to recording their thermograms to remove their previous thermal history and recorded using a heating/cooling rate of 10 °C/min under a purge of dry nitrogen. The liquid crystalline properties of the OPVs were investigated using Nikon HFX 35 A Optiphot 2-Pol polarized light optical microscope equipped with a Linkam THMS 600 heating and freezing stage connected to a Linkam TMS 93 temperature programmer. Fluorescence light microscopy (FLM) was done on a Nikon Eclipse E-600 using an

excitation filter EX-330−380, EX-410−450 nm, emission filter BA-400, and dichromatic mirror DM-400. LC frozen and powder X-ray diffraction patterns were recorded with a Philips analytical diffractometer using Cu Kα emission. The spectra were recorded in the range of $2\theta = 0-40$ and analyzed using X'pert software. Variable X-ray diffraction studies were performed using a Rigaku Dmax 2500 diffractometer with a copper target. The system consists of a rotating anode generator with a copper target and a wide-angle powder goniometer fitted with a high-temperature attachment. The generator was operated at 40 kV and 100 mA. All the experiments were performed in the reflection mode. The sample holder was a copper block, and the powder sample was filled in the block. The absorption and emission studies were done with a Perkin-Elmer Lambda 35 UV−visible spectrophotometer and Spex-Fluorolog DM3000F spectrofluorometer with a double grating 0.22-m Spex 1680 monochromator and a 450-W Xe lamp as the excitation source using the front-face mode. The solution spectra were recorded in THF, and for the solid-state spectra thin films (10−100 μM) were prepared by drop casting THF solution on glass substrates. The solution quantum yields of the OPVs were determined using quinine sulfate in 0.1 M H_2SO_4 ($\phi = 0.546$) as the standard. Photophysical properties of the liquid crystalline samples were investigated by freezing the samples in the LC state. The fluorescence lifetime was measured using an IBH FlouroCube time-correlated picosecond single photon counting system (TCSPC). Solutions and films were excited with a pulsed diode laser 401 nm, <100 ps pulse duration with a repetition rate of 1 MHz. The detection system consisted of a microchannel plate photomultiplier (5000U-09B, Hamamatsu) with a 38.6 ps response time coupled to a monochromator (5000M) and TCSPC electronics (Data Station Hub including Hub-NL, Nano LED controller, and preinstalled Fluorescence Measurement and Analysis Studio (FMAS) software). The fluorescence lifetime values were determined by deconvoluting the data with exponential decay using DAS6 decay analysis software. The quality of the fit was judged by fitting parameters such as $\chi^2 < 1$, as well as the visual inspection of the residuals.

The detailed synthesis of intermediate molecules and other OPVs and their structural data are provided as Supporting Information. Here we describe the detailed procedure for the synthesis of BTCD-BDD-OPV only.

Synthesis of 1,4-Bis(4-dodecyloxystyryl)-2,5-di(1,8-tricyclodecanemethyleneoxy)benzene (BTCD-BDD-OPV). 1,4-Bis(bromomethyl)-2,5-di(1,8-tricyclodecanemethyleneoxy)benzene (2.00 g, 3.4 mmol) and triethylphosphite (1.13 g, 6.8 mmol) were heated to 140−150 °C for 12 h under nitrogen atmosphere. Excess triethyl phosphite was removed by vacuum distillation, and the resultant ylide 1,4-bis(tricyclodecanemethyleneoxy)-2,5-xylenetetraethyldiphosphonate was obtained as a thick yellow oil. ^{1}H NMR ($CDCl_3$, 300 MHz) δ: 6.88 (t,2H, Ar-H), 4.06 (m, 8H, -PO-OCH_2), 3.68 (m, 4H, Ar-OCH_2), 3.24 (m, 4H, Ar-CH_2P), 1.69−1.21 (m, 42H, aliphatic). FT-IR (cm^{-1}): 3445, 2947, 2868, 1681, 1509, 1474, 1415, 1392, 1305, 1245, 1210, 1163, 1094, 1048, 1029,964, 894, 875, 831, 782, 729, 529 cm^{-1}. To the above crude product (0.53 g, 0.075 mmol) in 20 mL of dry THF were added 4-dodecyloxybenzaldehyde (0.55 g, 0.19 mmol) and potassium *tert*-butoxide (5 mL, 1 M THF), and the mixture was stirred under nitrogen for 24 h at 30 °C and then poured into methanol. The yellow precipitate formed was filtered and purified by passing through silica gel column using 2.5% ethyl acetate in hexane as eluent. Yield = 90%, mp = 160−161 °C. ^{1}H NMR ($CDCl_3$, 300 MHz) δ: 7.47−6.88 (m, 14H, Ar-H and vinylic H), 4.00−3.96 (t, 4H, Ar-OCH_2-DD), 3.83−3.75 (m, 4H, Ar-OCH_2-TCD), 2.41−0.86 (m, 76H, cyclic-H and aliphatic-H). ^{13}C NMR ($CDCl_3$, 75 MHz) δ: 158.6, 151.0, 130.6, 128.3, 127.5, 126.6, 121.4, 144.5, 110.9 (Ar-C), 73.5 (Ar-OCH_2-DD), 67.9 (Ar-OCH_2-TCD), 45.6, 45.2, 43.9, 41.2, 34.6, 31.8, 29.5, 29.3, 29.2, 28.9, 27.9, 26.9, 26.4, 25.9, and 22.6 (cyclic and aliphatic-C). FT-IR (cm^{-1}): 2919, 2850, 1606, 1575, 1511, 1489, 1475, 1423, 1381, 1291, 1243, 1190, 1176, 1008, 971 (HC═CH, trans), 852 (HC═CH, cis), 818, 720 cm^{-1}. HR-MS (MW 979.5): $m/z = 978.9$ (M^+). Anal. Calcd for $C_{68}H_{98}O_4$: C, 83.38; H, 10.08. Found: C, 83.02; H, 10.38.

Results and Discussion

Synthesis and Liquid Crystalline Properties. A series of OPVs based on TCD, 2-ethylhexyl, and dodecyl pendants were synthesized by following the Wittig−Horner reaction as shown in Scheme 1. The bis-alkoxy coupled product (**1**) was refluxed with HBr in acetic acid and *p*-HCHO to obtain the bisbromomethylated compound (**2**), which upon treatment with triethylphosphite yielded the corresponding ylide (**3**).[40,46] The ylide was then reacted with benzaldehyde or 4-dodecyloxybenzaldehyde to yield 10 different types of OPVs (see Scheme 1; more detailed structures are provided in Supporting Information). The structures of the OPVs were confirmed by ^{1}H NMR, ^{13}C NMR, FT-IR, elemental analysis, and HRMS (see Supporting Information). For simplicity, the OPVs were labeled as XXX-YYY-OPV, where XXX and YYY are corresponding to the alkoxy substitutions at the middle and outer phenyl groups, respectively. For instance, BTCD-BDD-OPV represents the bis-TCD substitution in the middle ring and dodecyl chains at the outer phenyl rings. The thermal stabilities of the OPVs were analyzed by TGA, and it was found that all OPVs exhibited good thermal stability with onset of degradation above 300 °C (see Figure 2 in Supporting Information). All OPVs were subjected to DSC to study the thermal transitions in the heating/cooling cycles. MEH-OPV, BEH-OPV, and MTCD-OPV were found to be sluggish to crystallize and were obtained as amorphous solids. BDD-OPV, MEH-BDD-OPV, BEH-BDD-OPV, and MTCD-BDD-OPV showed crystallization peaks and melting transitions in the cooling/heating cycles like normal crystalline solids (see Figure 3 in Supporting Information). BTCD-OPV, TDD-OPV, and BTCD-BDD-OPV showed typical DSC thermograms corresponding to thermotropic LC behavior. The DSC thermograms of these LC-OPVs are given in Figure 1, and the data are provided in Supporting Information. The DSC plot of the BTCD-OPV showed LC features upon cooling from the melt with two closely spaced exotherms corresponding to the isotropic−LC (162 °C) and LC−crystalline (156 °C) transitions. On subsequent heating two peaks were observed corresponding to weak crystal−LC (at 176 °C) and strong LC−isotropic (at 225 °C) transitions.[46] Tetradodecyl-substituted TDD-OPV showed LC behavior in the cooling/heating cycles, but the transitions were observed at a much lower temperature region (<100 °C) compared to that of BTCD-OPV. Interestingly, BTCD-BDD-OPV exhibited LC properties in the temperature range between their homocounterparts BTCD-OPV and TDD-OPV (see Figure 1). The LC temperature window (temperature range in which LC behavior is exhibited) in the cooling cycles was obtained as 6, 10 and 62 °C for the BTCD-OPV, TDD-OPV, and BTCD-BDD-OPV, respectively. Similarly, in the heating cycles the window was obtained as 56, 20 and 109 °C for the same OPV samples. The enthalpies of cooling and heating cycles (see Table 1 in Supporting Information) suggest that dodecyl substitution leads to less crystalline nature in the OPVs, and the trend was found to be decreasing in the order TDD-OPV < BTCD-BDD-

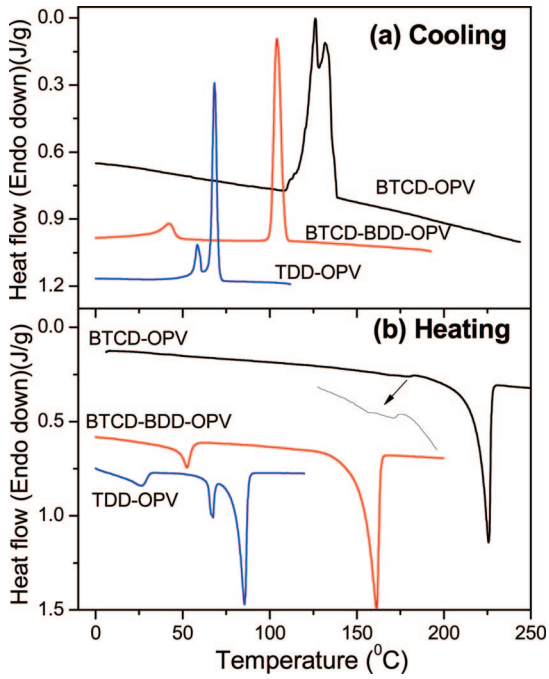

Figure 1. DSC thermograms of LC-OPVs under 10 °C/min heating and cooling.

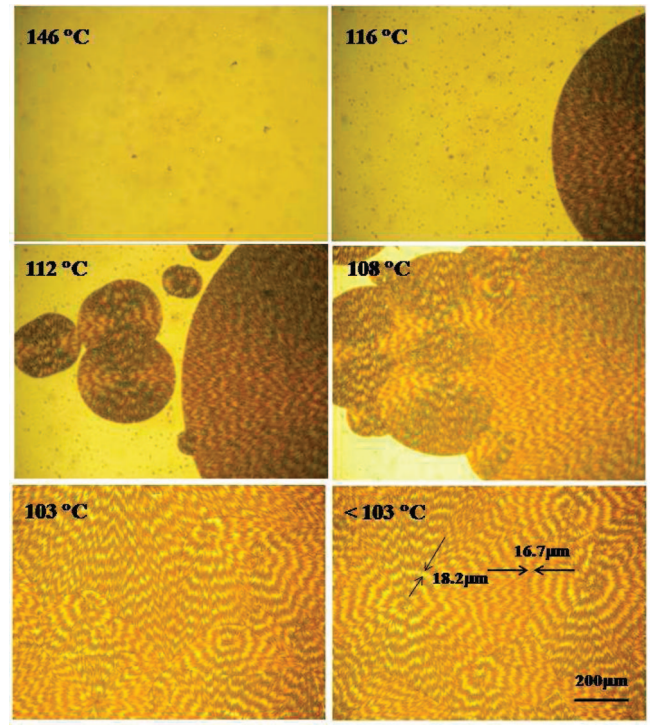

Figure 2. PLM images of BTCD-BDD-OPV at 10 °C/min cooling from melt.

OPV < BTCD-OPV. The overall DSC analysis revealed that BTCD-BDD-OPV was a very good LC material and possessed large LC temperature window both in cooling and heating cycles. It is very important to note that the LC behavior of OPVs is not easily predictable and is highly dependent on the type of rigid or flexible side chains attached on the middle and outer aromatic rings.

Liquid crystalline behavior of the OPVs was studied using a polarized light microscope (PLM) attached with a temperature programmable hot stage. All compounds were heated to melt at 10 °C/min, kept isothermally 20 °C above their isotropic temperature for 2−3 min, and subsequently cooled to room temperature at 10 °C/min. PLM images of BTCD-BDD-OPV are shown in Figure 2. While cooling from the melt, BTCD-BDD-OPV showed a rhythmic growth of spherulitic ring bands. The pattern grew slowly with decrease in the temperature, and the texture remained unchanged to room temperature. It is also important to note that with decrease in temperature new nucleating sites were also created and the crystal growth occurred in an almost identical ring banded pattern in all nucleating sites. The dark and bright bands in the PLM patterns are more like spiral rather than concentric rings. The band widths of the bright and dark bands were determined to be 18.2 (±1.0) and 16.7 (±1.8) μm, respectively. The images of the other two LC OPVs, BTCD-OPV and TDD-OPV, revealed that the narrow LC window (<10 °C) hampered the morphological development (see Figure 4 in Supporting Information). Because it was observed that the crystallization process from the melt was highly dependent on the cooling conditions, it is very important to study the effect of external cooling on the ring banded structure. To investigate the effect of cooling rates (non-isothermal) and crystallization residence time (isothermal), the sample was subjected to isothermal/non-isothermal crystallization process by both DSC as well as PLM. Non-isothermal crystallization was carried out at different cooling rates ranging from 2, 5, 8, 10, and 20 °C/min. The DSC plots as well as their thermal data are given as Supporting Information. PLM images of the BTCD-BDD-OPV under cooling rates at 2 and 20 °C/min are shown in Figure 3 (other data are given as Supporting Information). Each time fresh samples were loaded and the images were captured at 10X magnification for qualitative comparison of the data. At 2 °C/min, only one nucleating site could be observable (nucleated in a site away from the lens frame), and the layer of ring bands expanded with decrease in temperature. It is very important to note that no new nucleating site appeared until the end of crystallization. At higher cooling rates (20 °C/min), both new nucleating sites as well as the expansion of ring bands of existing ones were noticed. Isothermal crystallization was performed at different crystallization temperatures (T_c) of 115, 120, and 125 °C. The sample was rapidly cooled (30 °C/min) from the melt to the desired T_c and allowed to crystallize isothermally (T_c was chosen on the basis of DSC analysis; see Supporting Information). At T_c = 125 °C, crystallization starts after ~2 min and only a single nuclei was initiated. Over a period of time, the ring banded structures grew in the entire frame with multiple layers. At lower T_c = 115 °C, the samples produced a large number of nucleating sites and resulted in the formation of banded structures with fewer rings.

Various parameters from the above crystallization process, such as T_c, enthalpy of crystallization (ΔH_c) of isotropic-to-LC, number of nucleating sites, and average width of the dark and bright bands, were plotted against the cooling rates and are shown in Figure 4. The DSC data at different cooling rates (from 2 to 20 °C/min) indicate that both the ΔH_c and T_c decrease as a function of increase in cooling rate. The spherulites were less ordered with 3 to 4 ring bands at 20 °C/min compared to highly crystalline domains with larger ring banded structures at a slow cooling rate (at 2 °C/min). The number of nucleating sites (NS) increased with increase in cooling rates, which account for the less ordered crystalline domains (low enthalpy values). This can be explained as follows: at a slower cooling rate the melt experiences less stress by external stimuli and the slow crystal growth produces highly crystalline materials. A similar observa-

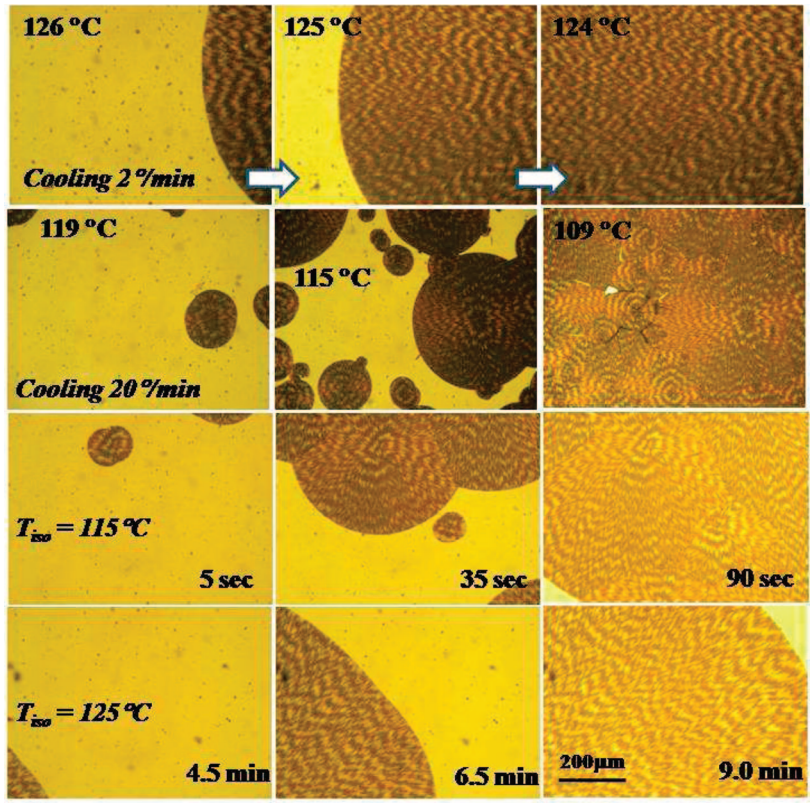

Figure 3. PLM images of BTCD-BDD-OPV in the non-isothermal (2 and 20 °C/min) and isothermal crystallization process from isotropic stage.

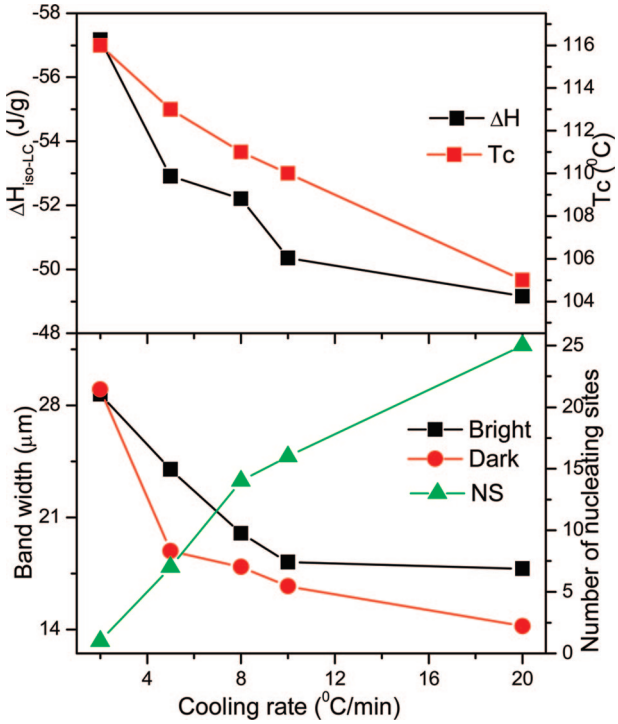

Figure 4. Plots of crystallization parameters with cooling rates (NS = nucleating sites).

tion could also be seen for the isothermal crystallization depending upon their T_c (see Figure 3 and DSC data in Supporting Information). As expected, at higher T_c, the sample follows the trend as observed at a slow cooling rate in the non-isothermal process. The average widths of the bands were calculated from the PLM images. The ring bandwidth increased with decrease in cooling rate, which suggested that at slow cooling rate the crystalline domains have a high tendency for alignment to produce thick ring bands. Therefore, using the current approach, one can pattern the conjugated crystalline molecules, particularly OPVs, either with large ring bands from single nucleation or multiple small rings depending upon the T_c or cooling rates employed in the isothermal or non-isothermal processes, respectively. Therefore, the ring banded structures observed in BTCD-BDD-OPV are not merely an artifact but rather a reproducible phenomena in the LC phase irrespective of the crystallization processes (isothermal or non-isothermal). These crystallization experiments indicated that one can pattern the OPV conjugated material with a desired number of rings by adapting different cooling rates or crystallizing at different T_c, which is very rarely reported in the literature. It is not possible to generalize that all OPV molecules will show ring banded morphology, since the LC window and crystallization phenomena of the OPVs are highly dependent on their structure.

Ring Banded Morphology. It is generally believed that ring-banded structures occur as a result of the periodic twisting of lamellar crystals along the radial growth direction of the spherulites.[11−13] To understand the mechanism of the ring banded structures in OPVs, an isothermally crystallized sample of BTCD-BDD-OPV at T_c = 120 °C was closely observed (see images in Figure 7 in Supporting Information). It is obviously clear from the images that the formation of ring banded spherulites can be noticed starting from the nucleation process. Two nucleation positions (sites 1 and 2, Figure 7 in Supporting Information) were clearly visible in the image, and site 1 was closely monitored to observe the ring structure formation. The nucleation occurs instantaneously and a needlelike crystal starts growing radially from the center. It forms disklike first stage bands around the nucleating site, and the ring bands expand with time (two, three rings, and so on). Typically, in the liquid crystalline sample, the molecules or group of molecules act as

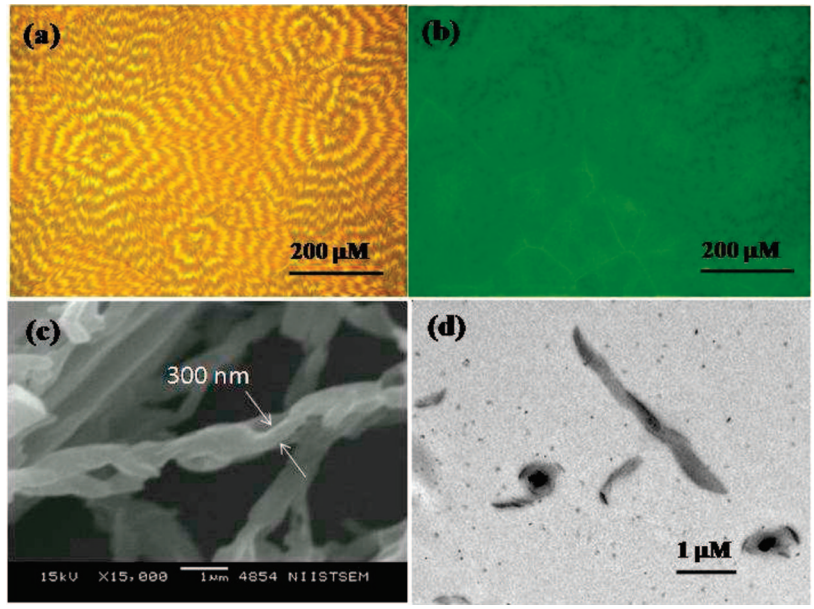

Figure 5. PLM (a), fluorescence light microscopic (b), SEM (c), and TEM (d) images of LC frozen BTCD-BDD-OPV.

mesogens, which facilitate molecular orientation in LC phase.[39] Therefore, the continuous upward diffusion of mesogens to the front crystalline phase creates depletion regions (valleys). The artificial density gradient arising from the movement of mesogens further facilitates the movement of more molecules far from the growth site for the formation of the second ring band.[16] This process repeats as many times as possible with alternative ridge and valleys until interrupted by the neighboring crystal growth (in this case site 2). The size of the banded spherulites is in the micrometer range, and therefore the samples were subjected to SEM and TEM analysis for understanding the nucleation and growth. For SEM analysis, the sample was prepared in hot stage (at 10 °C/min) under the polarizing microscope and a portion of the sample (with ring banded structures) was carefully transferred into the SEM grid. The sample for TEM analysis was prepared by placing a pinch of sample on a Formvar coated TEM grid in a DSC pan and subjected to heating/cooling cycles as shown in Figure 1. SEM and TEM images of the samples are shown in Figure 5. The SEM image of the LC frozen sample has 300 nm wide and few micrometers long twisted and aggregated micrometer size crystals. Closer observation of the twist revealed that the microcrystals are self-organized and twisted along the axis of the rotation. The average width of the crystals was determined as 230−300 nm with length up to 0.4−0.5 μM. The TEM image of the LC frozen sample also confirmed the presence of twisted microcrystalline solids. The contrast difference along the axis of the aggregated crystals also confirmed the helical phase orientation of the crystals. Electron microscopic images provide direct evidence for the twisted helical assemblies of micrometer size crystals. The long-range ordering of these helical (or twisted) assemblies (at submicrometer level) leads to the formation of supra-ring structures in the PLM image (at 20 μM level). Although both electron microscope techniques confirmed the existence of twisted crystalline alignments in the band ring spherulites, the lamellar twisting at molecular (or mesogen) level could not be observed because of size limitations.

To identify the lamellar mesophases, the sample BTCD-BDD-OPV was subjected to X-ray diffraction analysis in powder, LC frozen state, and at variable temperatures. The X-ray diffraction patterns of the powder and LC frozen samples are shown in

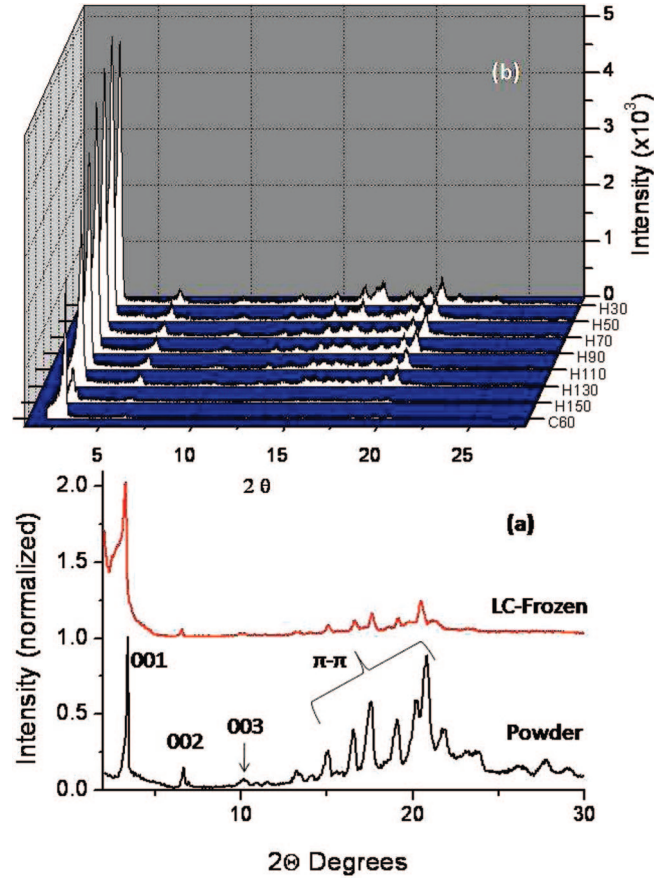

Figure 6. X-ray diffraction pattern of BTCD-BDD-OPV at 30 °C (a) and at variable temperatures (b).

Figure 6a. The powder sample showed multiple sharp crystalline peaks corresponding to a highly crystalline state. A bunch of peaks appeared in the higher angle region from $2\theta = 15-25$ ($d = 4-6$ Å), which corresponds to aromatic ring packing.[49,50] In the low angle region ($2\theta > 15$), three peaks at $2\theta = 3.26$, 6.32, and 10.0 were clearly visible. The d-spacing values of these reflections corresponded to 27.07, 13.97, and 8.90 Å with regular periodicity. The highly intense sharp peak at 27.07 Å was assigned to the fundamental 001 plane of the lamellar

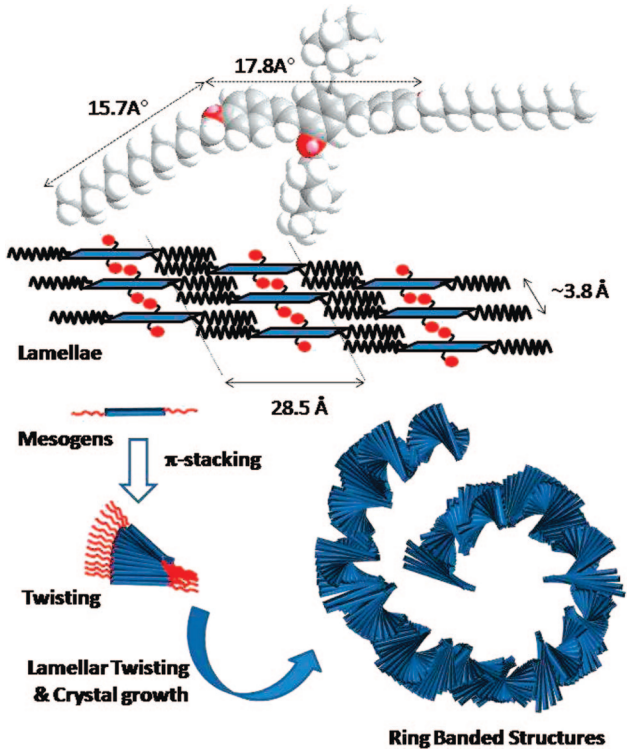

Figure 7. Energy-minimized structure of BTCD-BDD-OPV and mechanism for the ring banded suprastructures.

structure, and other two less intense peaks at 13.97 and 8.90 Å were assigned to higher order reflections 002 and 003, respectively, in the lamellae.[30] The presence of these fundamental peaks at the low angle region proved the existence of the lamellar structure in the molecule. The sample was heated to melt (T_m = 160 °C) and subsequently cooled at 10 °C/min to obtain ring banded structures (confirmed by PLM). The frozen LC sample was also subjected to X-ray analysis, and the pattern is shown in Figure 6a. After melt crystallization, the intensity of the peaks at higher angle region was reduced significantly; however, the fundamental reflections at the lower angle region were unaltered. The sample was further subjected to variable temperature X-ray analysis heating/cooling from 30 to 170 °C in the LC active temperature window. Upon heating (see Figure 6b), the crystalline peaks slowly started to disappear. In the isotropic region (160−170 °C), the sample was completely melted and all crystalline peaks vanished. In the subsequent cooling cycle, the three original fundamental peaks reappeared at 28.5, 14.0, and 8.90 Å. The first order peak observed in the variable temperature X-ray analysis was ~1.5 Å higher than with the power sample, but this difference falls within the experimental error limit. These detailed X-ray analyses revealed that the lamellar structure in the molecule is reproducible in repetitive heating/cooling conditions.

All of our attempts to grow a single crystal of the BTCD-BDD-OPV molecule have not been successful so far (attempts are still ongoing), and therefore the energy minimization for the molecular structure was traced using Chem Bio 3D ultra 11.0. The bulky TCD units in the central aromatic rings occupy both sides of the conjugated backbone and the long alkyl chain project from the outer phenyl rings. The dimensions of BTCD-BDD-OPV were obtained from the energy-minimized structure and are shown in Figure 7. A model for the BTCD-BDD-OPV molecular packing was constructed on the basis of the energy-minimized structure, fundamental lamellae reflections in the X-ray diffractions, and electron microscopic images (see Figure 7). The rigid central aromatic core and long alkoxy chains makes these molecules behave as typical liquid crystalline mesogens. The close packing of these mesogens creates lamellar structures with spacing of 28.5 Å (based on the *d*-spacing for the first sharp fundamental reflection at 2θ = 3.16; see Figure 6) and gives evidence for the existence of lamellar structures in the liquid crystalline BTCD-BDD-OPV. The interlamellae distance is expected to be equal to 33.5 Å on the basis of the molecular structure calculation (17.8 + 15.7 Å); however, we could observe peaks only at 28.5 Å in the wide-angle X-ray diffractions. There is a difference of ~5 Å between the theoretical structure and experimentally determined values. This is because wide-angle X-ray has limitations in resolving the peaks at the very low angle region ($2\theta < 2.0$). The interlayer distance in the aromatic core was 2θ = 15−25 (d = 4−6 Å), which is much larger than that reported for π-stacking.[49,50] This may be due to the presence of two large bulky TCD units positioned at either side of the π-conjugated backbone. Usually the aromatic π-core interactions are expected in the range of 3.0 Å;[25] however, recently Gill et al.[51] reported a much larger interlayer distance (3.77 Å) in their octyloxy-substituted OPVs due to strong steric hindrance. Therefore, it may be assumed that TCD is much bulkier than octyloxy pendants and therefore would be expected to show more steric hindrance leading to a larger interlayer distance of ~4 Å in BTCD-BDD-OPV. However, more structure analysis such as single crystal study is required to confirm the above observation. Nevertheless, wide-angle X-ray analysis data had been widely utilized to calculate the interlayer distance in self-assembled systems, and therefore, the interlayer distances reported here also should be acceptable. On the basis of the above data and morphological analysis of LC phases by PLM, SEM, and TEM, we postulate the following mechanism for ring banded structures in OPV as shown in Figure 7. The following steps are involved in the formation of ring banded structures: (i) the crystallization starts from nucleation (evident from Figures 2 and 3), (ii) BTCD-BDD-OPV mesogens self-organized to form lamella (evident from XRD), (iii) the strong aromatic interactions in the OPV backbone induced long-range twisted lamellar aggregates that result in the growth of helical microcrystalline arrangements (evident by SEM and TEM), and (iv) the ring-banded structures in PLM are the consequent diffusion of these microcrystalline domains in the LC phase to the crystal front. Comparison of the sizes of the molecular mesogens (from XRD, width = ~28.5 Å = 2.85 nm) and ring banded structures (from PLM, width = ~20 μM) revealed that each ring may contain more than 100−1000 molecules in the width and millions in the twisted length. Therefore, the formation of ring banded structures in the current system has originated from the molecular aggregation of the mesogens, which leads to macroscopically banded structures. The present investigation directly provides experimental evidence for the mechanism proposed by Keith and Padden, i.e., "the ring banded structure was attributed to periodic twisting of lamellar crystals along the radical growth direction of the spherulites".[5−9] To our knowledge, these are the first ring banded structures observed in any type of conducting material. The ring banded structure is an exception and not the rule in OPVs, since its formation highly depended on the chemical structure of the π-conjugated backbone.

Photophysical Studies. Unlike other banded ring structures[3,4,14] in the present system, the LC mesogen bears a photoactive OPV conjugated unit, and therefore photophysical characterization such as excitation, emission, and fluorescence decay profile can be employed as tools to trace the π-stacking phenomena at the

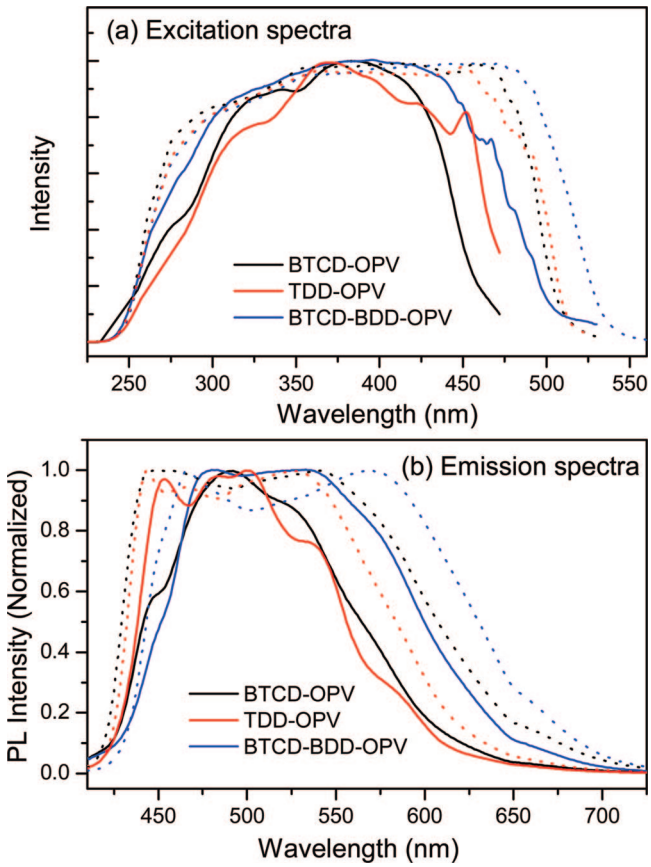

Figure 8. Excitation and emission (excited at 400 nm) spectra of BTCD-BDD-OPV: film with 0.1 OD (solid line) and LC frozen (dotted line).

lamellar structures (at the molecular level). Photophysical properties of the OPVs were studied in solution (in THF; see Figure 8 in Supporting Information), solvent cast film, and also LC frozen solids. Solid films of the OPVs were cast on the glass plate, and the emission and excitation spectra of the BTCD-OPV, TDD-OPV, and BTCD-BDD-OPV are given in Figure 8. The excitation and emission spectra of the BTCD-BDD-OPV in film (see Figure 8a and b) were red-shifted almost 40 nm compared to BTCD-OPV and TDD-OPV. The small peak at 452 nm in the excitation spectrum of TDD-OPV corresponds to the influence of -OR groups on the OPV absorption (see other examples in Figure 9 in Supporting Information). The BTCD-BDD-OPV also showed an additional peak at 470 nm in the excitation spectrum corresponding to the presence of strong π-aggregation. The excitation spectra of LC frozen samples showed further red-shift compared to films, and the shift was found to be much larger for BTCD-BDD-OPV compared to all of the samples. A thin layer of ring banded structures were prepared on a glass plate for BTCD-BDD-OPV by heating/cooling under the PLM (similarly for BTCD-OPV and TDD-OPV). The sample was subjected to fluorescence microscopic analysis with excitation light source at 420−450 nm. The FL microscope image is shown in Figure 5b. The ring banded morphology appeared green as a result of the emission color of the OPV units. It is clearly evident that the ring banded structures are luminescent under photoexcitation. The emission spectra of film and LC frozen samples of BTCD-BDD-OPV were found largely red-shifted (as noticed in the excitation spectra) and provide additional proof for strong π-aggregation compared to other OPVs. It is well-known that the molecular aggregation in π-conjugated chains are expected to quench the luminescence.[53,54] Therefore, one would expect a significant difference in the emission decay profile among these samples. Time-dependent fluorescence decay measurements for BTCD-BDD-OPV and BTCD-OPV films were carried out by exciting with 401 LED laser light source. The fluorescence decay profiles (see Figure 10 in Supporting Information) revealed that the strongly aggregated BTCD-BDD-OPV molecules showed a faster decay profile compared to that of BTCD-OPV. The lifetime values were obtained as $\tau_1 = 0.18$ ns and $\tau_2 = 1.25$ ns for BTCD-BDD-OPV and $\tau_1 = 1.25$ ns and $\tau_2 = 4.02$ ns for BTCD-OPV.[55] The highly aggregated BTCD-BDD-OPV showed faster fluorescence decay with shorter lifetime compared to weakly aggregated BTCD-OPV. More detailed studies using optically active side chains in the BTCD-OPV mesogens will provide more insight into the twisting phenomena. We are currently engaged in making such molecules, and the results will be published elsewhere. It is very important to add that the proposed mechanism for the ring banded structures is very suitable for OPVs and also for other types of conjugated materials but may not be relevant to commercial thermoplastic polymers such as polyesters. It is also not possible to rule out the fact that a similar molecular interaction at the lamellar level may also exist in systems such as polyesters; however, the lack of availability of optical probes like OPV limit their fundamental understanding. The approach reported here for patterning of ring banded morphology may be attractive because the conjugated materials can be easily aligned or self-organized in micrometer range for optoelectronics on a solid support without being subjected to tedious processes such as high temperature vacuum deposition techniques, etc. Additionally, the melt crystallization process is solvent-free, and therefore the solubility parameters of the materials in organic solvents may not restrict their processability. In a nut shell, in the present investigation, for the first time, we have successfully utilized aromatic π-interactions as a self-organization tool to produce supramolecular ring banded structures, particularly in a LC oligo(phenylenevinylene).

Conclusion

In conclusion, we have designed and developed a series of bulky conjugated oligo(phenylenevinylene)s for tracing the role of structure on the thermotropic liquid crystalline behavior. Among all of the examples, BTCD-BDD-OPV was found to show a unique ring banded morphology. The most important findings in the current approach may be listed as follows: (i) the structure of π-conjugated backbone is very crucial for long-range lamellae ordering of liquid crystalline mesogens for ring banded morphology, (ii) the lamellar aggregation of the OPV molecules produces sharp peaks in the X-ray diffraction patterns at the low angle region that were reproducible in repetitive heating/cooling cycles, (iii), the long-range amplitude of the lamellar twisting can be observed in the electron microscopic images as helically self-organized microcrystals, (iv) the nature of the ring banded morphological development is less influenced by the non-isothermal or isothermal crystallization process although these conditions influence the number of rings or layers in each spherulites, (v) luminescent ring banded structures can be obtained by exciting the OPVs with a suitable light source, (vi) photophysical experiments such as excitation, emission, and time-dependent fluorescence decay were successfully utilized to prove the existence of strong $\pi-\pi$ interactions in the OPVs that behave as a main driving force for the self-organization process, (vii) size and shape of the pendants attached in the OPV backbone are crucial factors for inducing liquid crystalinity and also tuning wide LC temperature window, (viii) tricyclo-

decanemethanol is proven to be an effective structure directing unit for LC phases compared to that of normal alkyl chains, and (ix) the current system directly provides experimental evidence of the lamellar twisting mechanism proposed by Keith and Padden based on computational simulation and microscopes. Here we have successfully shown a new way to pattern micrometer range ring structures via melt crystallization process, which is expected to be a very attractive and clean way to produce electronically important OPV-based conjugated materials. The approach could be expanded for a wide range of other classes of conjugated materials and may open new opportunities for patterning and understanding the self-organization behavior of conjugated segments through melt crystallization processes.

Acknowledgment. We thank the Department of Science of Technology, New Delhi, India under Scheme NSTI Programme-SR/S5/NM-06/2007 for financial support. The authors thank Dr. Peter Koshy, Mr. M. R. Chandran, Dr. U. Syamaprasad, and Mr. P. Gurusamy, NIIST-Trivandrum for SEM, TEM, and WXRD analysis. We also thank Dr. C. Ramesh, NCL-Pune for temperature-dependent X-ray analysis. S.R.A. thanks CSIR-New Delhi, India for a senior research fellowship.

Supporting Information Available: ^{1}H NMR and HRMS spectra, synthesis and structural details, TGA plots, DSC thermogram of the non-LC OPVs, enthalpy, bandwidth and number of nucleating sites in the non-isothermal and isothermal crystallization process of the OPVs, GPC data, PLM images of BTCD-OPV and TDD-OPV, non-isothermal and isothermal DSC thermograms, energy-minimized models of the OPVs, excitation spectra and fluorescence decay profiles of the OPVs in the film. Intensity versus concentration plot, concentration-dependent ^{1}H NMR and photophysical studies are also provided. This material is available free of charge via the Internet at http://pubs.acs.org.

References and Notes

(1) Mandelkern, L. *Crystallization of Polymers*; McGraw-Hill: New York, 1964.

(2) (a) *Handbook of Liquid Crystals*; Demus, D., Goodby J. W., Gray, G. W., Spiess, H.-W., Vill, V., Eds.; Wiley-VCH: Weinheim, 1998. (b) *Thermotropic Liquid Crystals*; Gray, G. W., Ed.; Wiley: Chichester, 1987.

(3) Chen, J.; Yang, D. *Macromolecules* **2005**, *38*, 3371.

(4) Hutter, J. L.; Bechhoefer, J. *J. Cryst. Growth* **2000**, *217*, 332.

(5) Keith, H. D.; Padden, F. J., Jr. *J. Polym. Sci.* **1958**, *31*, 415.

(6) Keith, H. D.; Padden, F. J., Jr. *J. Polym. Sci.* **1959**, *39*, 101.

(7) Keith, H. D.; Padden, F. J., Jr. *J. Polym. Sci.* **1959**, *39*, 123.

(8) Keith, H. D.; Padden, F. J.; Russel, T. P. *Macromolecules* **1989**, *22*, 666.

(9) Keith, H. D.; Padden, F. J., Jr. *Polymer* **1984**, *25*, 28.

(10) (a) Keller, A. *J. Polym. Sci.* **1955**, *17*, 351. (b) Keller, A. *J. Polym. Sci.* **1959**, *39*, 151.

(11) Price, F. P. *J. Polym. Sci.* **1959**, *39*, 139.

(12) Keller, A. *Nature (London)* **1952**, *31*, 913.

(13) (a) Wang, B.; Li, C. Y.; Hanzlicek, J.; Cheng, S. Z. D.; Geil, P. H.; Grebowicz, J.; Ho, R. M. *Polymer* **2001**, *42*, 7171. (b) Gazzano, M.; Focarete, M. L.; Riekel, C.; Ripamonti, A.; Scandola, M. *Macromol. Chem. Phys.* **2001**, *202*, 1405.

(14) Ho, R. M.; Ke, K. Z.; Chen, M. *Macromolecules* **2000**, *33*, 7529.

(15) Wang, Y.; Chan, C. M.; Li, L.; Ng, K. M. *Langmuir* **2006**, *22*, 7384.

(16) Wang, Z.; Hu, Z.; Chen, Y.; Gong, Y.; Huang, H.; He, T. *Macromolecules* **2007**, *40*, 4381.

(17) Chen, J.; Yang, D. *J. Polym. Sci., Part B: Polym. Phys.* **2007**, *45*, 3011.

(18) Okabe, Y.; Kyu, T.; Saito, H.; Inoue, T. *Macromolecules* **1998**, *31*, 5823.

(19) Xu, J.; Guo, B. H.; Zhou, J. J.; Li, L.; Wu, J.; Kowalczuk, M. *Polymer* **2005**, *46*, 9176.

(20) Cheung, Z. L.; Weng, L. T.; Chan, C. M.; Hou, W. M.; Li, L. *Langmuir* **2005**, *21*, 7968.

(21) (a) El-ghayoury, A.; Schenning, A. P. H. J.; van Hal, P. A.; van Duren, J. K. J.; Janssen, R. A. J.; Meijer, E. W. *Angew. Chem., Int. Ed.* **2001**, *40*, 3660. (b) Precup-Blaga, F. S.; Garcia-Martinez, J. C.; Schenning, A. P. H. J.; Meijer, E. W. *J. Am. Chem. Soc.* **2003**, *125*, 12953.

(22) Kato, T.; Mizoshita, N.; Kishimoto, K. *Angew. Chem., Int. Ed.* **2006**, *45*, 38.

(23) Eckert, J. F.; Nicoud, J. F.; Guillon, D.; Nierengarten, J. F. *Tetrahedron Lett.* **2001**, *41*, 6411.

(24) Hoeben, F. J. M.; Jonkheijm, P.; Meijer, E. W.; Schenning, A. P. H. J. *Chem. Rev.* **2005**, *105*, 1491.

(25) Hunter, C. A.; Lawson, K. R.; Perkins, J.; Urch, C. J. *J. Chem. Soc., Perkin Trans.* **2001**, *2*, 651.

(26) Yagai, S.; Kubota, S.; Iwashima, T.; Kishikawa, K.; Nakanishi, T.; Karatsu, T.; Kitamura, A. *Chem. Eur. J.* **2008**, *14*, 5246.

(27) Kato, T; Mizoshita, N.; Kanie, K. *Macromol. Rapid Commun.* **2001**, *22*, 797.

(28) Hoag, B. P.; Gin, D. L. *Liq. Cryst.* **2004**, *31*, 185.

(29) (a) Schenning, A. P. H. J.; El-ghayoury, A.; Peeters, E.; Meijer, E. W. *Synth. Met.* **2001**, *121*, 1253. (b) Gu, T.; Accorsi, G.; Armaroli, N.; Guillon, D.; Nierengarten, J. F. *Tetrahedron Lett.* **2001**, *42*, 2309.

(30) Campidelli, S.; Deschenaux, R.; Eckert, J. F.; Guillon, D.; Nierengarten, J. F. *Chem. Commun.* **2002**, 656.

(31) Camerel, F.; Donnio, B.; Bourgogne, C.; Schmutz, M.; Guillon, D.; Davidson, P.; Ziessel, R. *Chem. Eur. J.* **2006**, *12*, 4261.

(32) (a) George, S. J.; Ajayaghosh, A.; Jonkheijm, P.; Schenning, A. P. H. J.; Meijer, E. W. *Angew. Chem., Int. Ed.* **2004**, *43*, 3422. (b) Ajayaghosh, A.; Praveen, V. K. *Acc. Chem. Res.* **2007**, *40*, 644.

(33) Li, A. K.; Yang, S. S.; Jean, W. Y.; Hsu, C. S.; Hsieh, B. R. *Chem. Mater.* **2000**, *12*, 2741.

(34) O'Neill, M.; Kelly, S. M. *Adv. Mater.* **2003**, *15*, 1135.

(35) Nolde, F.; Pisula, W.; Müller, S.; Kohl, C.; Müllen, K. *Chem. Mater.* **2006**, *18*, 3715.

(36) Kim, J.; McQuade, D. T.; McHugh, S. K.; Swager, T. M. *Angew. Chem., Int. Ed.* **2000**, *39*, 3868.

(37) He, F.; Xu, H.; Yang, B.; Duan, Y.; Tian, L.; Huang, K.; Ma, Y.; Liu, S.; Feng, S.; Shen, J. *Adv. Mater.* **2005**, *17*, 2710.

(38) (a) Precup-Blaga, F. S.; Schenning, A. P. H. J.; Meijer, E. W. *Macromolecules* **2003**, *36*, 565. (b) Pisula, W.; Tomovic, Z.; Wegner, M.; Graf, R.; Pouderoijen, M. J.; Meijer, E. W.; Schenning, A. P. H. J. *J. Mater. Chem.* **2008**, *18*, 2968.

(39) Hulvat, J. F.; Sofos, M.; Tajima, K.; Stupp, S. I. *J. Am. Chem. Soc.* **2005**, *127*, 366.

(40) Jonkheijm, P.; Schoot, V. D. P.; Schenning, A. P. H. J.; Meijer, E. W. *Science* **2006**, *313*, 80.

(41) Maddux, T.; Li, W.; Yu, L. *J. Am. Chem. Soc.* **1997**, *119*, 844.

(42) Strehmel, B.; Sarker, A. M.; Malpert, J. H.; Strehmael, V.; Seifert, H.; Neckers, D. C. *J. Am. Chem. Soc.* **1999**, *121*, 1226.

(43) Olsen, B. D.; Jang, S. Y.; Luning, J. M.; Segalman, R. A. *Macromolecules* **2006**, *36*, 4469.

(44) Bao, Z.; Amundson, K. R.; Lovinger, A. J. *Macromolecules* **1998**, *31*, 8647.

(45) Amrutha, S. R.; Jayakannan, M. *J. Phys. Chem. B* **2006**, *110*, 4083.

(46) Amrutha, S. R.; Jayakannan, M. *Macromolecules* **2007**, *40*, 2380.

(47) (a) Amrutha, S. R.; Jayakannan, M. *J.Phys. Chem. B.* **2008**, *112*, 1119. . (b) Resmi, R.; Amrutha, S. R.; Jayakannan, M. *J. Polym. Sci. Polym. Chem.* **2009**, *47*, . in press.

(48) Thompson, B. C.; Kim, Y. G.; McCarley, T. D.; Reynolds, J. R. *J. Am. Chem. Soc.* **2006**, *128*, 12714.

(49) Ziessel, R.; Pickaert, G.; Camerel, F.; Donnio, B.; Guillon, D.; Cesario, M.; Prange, T. *J. Am. Chem. Soc.* **2004**, *126*, 12403.

(50) (a) Brouwer, H. J.; Krasnikov, V. V.; Pham, T. A.; Gill, R. E.; van Hutten, P. F.; Hadziioannou, G. *Chem. Phys.* **1998**, *227*, 65. (b) Resel, R.; Tertinek, B.; Tasch, S.; Davey, A.; Blan, W.; Horhold, H. -H.; Rost, H.; Leising, G. *Synth. Met.* **1999**, *101*, 96.

(51) Gill, R. E.; Meetsma, A.; Hadziioannou, G. *Adv. Mater.* **1996**, *8*, 212.

(52) Gill, R. E.; Hilberer, A.; van Hutten, P. F.; Berentschot, G.; Werts, M. P. L.; Meetsma, A.; Wittmann, J. C.; Hadziioannou, G. *Synth. Met.* **1997**, *84*, 637.

(53) (a) Chen, S. H.; Su, A. C.; Chou, H. L.; Peng, K. Y.; Chen, S. A. *Macromolecules* **2004**, *37*, 167.

(54) Hsu, J. H.; Fann, W.; Tsao, P. H.; Chuang, K. R.; Chen, S. A. *J. Phys. Chem. A* **1999**, *103*, 2375.

(55) (a) Jakubiak, R.; Collison, C. J.; Wan, W. C.; Rothberg, L. J.; Hsieh, B. R. *J. Phys. Chem. A* **1999**, *103*, 2394. (b) Fakis, M.; Anestopoulos, D.; Giannetas, V.; Persephonis, P. *J. Phys. Chem. B* **2006**, *110*, 24897.

JP809994T